JOURNAL OF Materials CHEMISTRY

Preparation and characterisation of silver quantum dot superlattice using self-assembled monolayers of pentanedithiol

Sushama Pethkar,[a] M. Aslam,[a] I. S. Mulla,[a] P. Ganeshan[b] and K. Vijayamohanan*[a]

[a]*Physical/Materials Chemistry Division, National Chemical Laboratory, Pune 411 008, India. E-mail: viji@ems.ncl.res.in; Fax: 0091-020-5893044*
[b]*Low Temperature Lab., Inter University Consortium for DAE Facilities, Indore 452 001, India*

Received 22nd November 2000, Accepted 13th March 2001
First published as an Advance Article on the web 9th April 2001

A superlattice of silver nanoclusters was prepared using sequential self-assembly of 1,5-pentanedithiol on an Au(111) substrate. The formation of highly ordered silver nanocluster arrays was confirmed using AFM and also by the longitudinal periodicity observed in the low angle X-ray diffraction pattern. In contrast to the behaviour of dithiol self-assembled monolayers (SAM) on gold substrates, which give only blocking behaviour, the superlattice exhibits interesting electrochemical properties in terms of redox accessibility of silver nanoclusters with respect to potential cycling. The room temperature emission spectrum suggests the formation of minibands in the superlattice structure as evidenced by three distinct peaks at 320, 400 and 620 nm.

I. Introduction

Different methods of organising quantum dot superlattices of metals and semiconductors have received significant interest in recent times as the tailoring of particle sizes and interparticle separation can, in principle, cause unique magnetic, optical and electronic behaviour.[1–5] For example, several nanocluster assemblies organised in different length scales have been found to be promising due to their potential applications in many diverse areas such as optoelectronic devices, single electron transistors and chemical sensors.[4–8] One of the principal objectives is to accomplish the design of broadly applicable synthetic schemes that produce superlattices of nanoparticles where the particle size as well as the interparticle coupling can be controlled.[9]

Self-assembled monolayer (SAM) formation offers a simple and flexible method for organising nanoclusters on noble metal surfaces and there have been several attempts recently to obtain a systematic arrangement of metal and semiconductor nanoparticles in different dimensions. Self-organised 2-D nanoparticle superlattices of semiconductors[10,11] and metals[12–15] as well as 3-D assemblies of nanoparticles[16,17] have been constructed and analysed. One of the important advantages of this approach is that the tailoring of band structure can be accomplished by selecting appropriate organic molecules to protect nanoclusters. Since many metallic and semiconducting clusters (Au, Ag, CdS, CdSe *etc.*) have high affinity for amine and thiol moieties, both the size and the interparticle separation can be controlled by changing the organic spacer. While it has been generally proved that both Ag and Au nanoclusters can be organised on a SAM surface, the sequential extension of this organisation to demonstrate novel optical and electrochemical properties is rather unknown. More significantly, the presence of organic ligands on the cluster surface can lead to considerable disorder in the superlattice formation and it is important to know if a sequential approach can be adopted to extend the organisation of superlattices of different cell parameters. Two-dimensional organisation of these clusters requires the control of the interparticle coupling and in comparison with semiconductors, metal clusters have strong dispersion interactions.[18] The nature of these interactions is indicative of the dependence of superlattice formation on particle size and also the degree of interparticle coupling through the bridging ligand.

In the present study, we have fabricated layer-by-layer self-assembly of ordered uncapped silver nanoclusters using a 1,5-pentanedithiol SAM as a building block on a gold substrate. More specifically, the role of the protective monolayer coating in controlling both the particle–particle interaction and the electron transfer properties of Ag clusters is investigated using X-ray diffraction (XRD), photoluminescence and electrochemistry after repeated SAM formation and cluster organisation. Although superlattices of alkanethiolate passivated silver nanoclusters have been reported earlier,[18,19] this is the first report of a repeated multilayer superlattice with photoluminescence and electrochemical characterisation.

II. Experimental

Vacuum deposited 200 nm Au (purity 99.99%) film was prepared using the procedure described previously.[20] The preferred orientation was found to be (111) by XRD. 1,5-Pentanedithiol, $AgNO_3$ and $NaBH_4$ obtained from Aldrich were used as received. In all the experiments deionized water from the Milli-Q system was used. The layer-by-layer formation of a silver quantum dot superlattice on a SAM surface was carried out in the following manner.

A SAM of 1,5-pentanedithiol was formed on an Au surface from a 1 mM ethanolic solution of the respective compounds for 24 h, followed by washing with ethanol and drying in a jet of argon. The details of the preparation and characterisation of these dithiol monolayers have been reported earlier.[21] The SAM covered gold surface was then introduced into a dilute aqueous dispersion of uncapped silver nanoclusters, instantaneously prepared by the controlled reduction of 10^{-4} M aqueous $AgNO_3$ solution using the desired amount of $NaBH_4$ by following reported procedures.[22] After the adsorption of silver particles (typically for 2 h), the substrate was washed with ethanol and dried in air. The second layer of dithiol SAM was formed by immersing this substrate in an

 DOI: 10.1039/b009372f

ethanolic solution of 1,5-pentanedithiol for several hours followed by subsequent adsorption of silver clusters as explained before. These steps were repeated to obtain multilayer superlattices of two and four layers of silver clusters (hereafter specified as 2L and 4L respectively). The self-assemblies thus prepared were characterised by low angle XRD, cyclic voltammetry (CV), AFM and photoluminescence.

The presence of metal nanoclusters in the initial solution was analysed using optical absorption spectrophotometry. The absorption spectra were recorded on a Hewlett Packard 8452 diode array spectrophotometer with 2 nm spectral resolution at room temperature.

SAM formation on the gold substrate was confirmed by XPS studies. The XPS measurements were performed on a VG Scientific ESCA-3 MK II spectrometer operated at a pressure of 10^{-9} Torr using a monochromatic MgKα source ($h\nu = 1253.6$ eV). The core level spectra of the C 1s and S 2p orbitals were recorded with an overall instrumental resolution of ~ 1 eV. The alignment of the binding energy was done using the Au 4f binding energy of 84 eV as reference. The X-ray flux was kept low to reduce beam-induced damage (electron power 70 W).

The assembly of silver cluster arrays on the SAM coated gold surface was identified by AFM imaging under ambient conditions using a Nanoscope II (Digital Instruments, USA) in the tapping mode. The AFM was initially calibrated using mica and then using a gold coated Si wafer. The first layer of the nanocluster arrays grown on the Au coated Si wafer was used for actual imaging. Silicon tip cantilevers with a force constant of 20–100 N m^{-1} and a resonance frequency around 200–400 kHz were used. The nominal tip radius was <10 nm. The AFM tip was guided to the middle of the sample before imaging. The images presented contain 256×256 data points collected within several seconds. The images were scanned from different areas of the sample to verify continuity in the structure. The error estimates on the horizontal and vertical distances were ± 0.1 Å and ± 0.05 Å respectively. To avoid tip-related artefacts, imaging was performed with minimal (up to 7 nN) force.

X-Ray diffraction (XRD) measurements were performed at room temperature using a Rigaku miniflex with filtered CuKα radiation ($\lambda = 1.5404$ Å). The scanning 2θ range was set between 1.5° and 5° at a scan rate of 0.5° min^{-1}.

Cyclic voltammograms were obtained using a Scanning Potentiostat Model 362 and a Recorder Model RE0151 using a standard three electrode cell comprising Ag nanoclusters organised on a gold substrate as the working electrode, a platinum foil as the counter electrode and a saturated calomel reference electrode (SCE) as reported earlier.[21] The scans were recorded with an instrumental accuracy of ± 1 mV and ± 5 μA.

Photoluminescence (PL) measurements were performed on a Perkin-Elmer (LS50) photoluminescence spectrophotometer. The emission spectra were collected between 300–800 nm using a 250 nm excitation and a 290 nm filter with a spectral resolution of ± 3 nm at room temperature.

III. Results and discussion

III.1 Optical absorption of silver hydrosol

Since the majority of the reported procedures for Ag cluster preparation use either capping agents or surfactants for the stabilisation of clusters in solution, it is extremely important to characterise the uncapped Ag cluster solution prior to the adsorption on the SAM surface. Fig. 1a illustrates the optical absorption spectra of the as-prepared cluster solution along with similar data obtained after 150 (Fig. 1b) and 270 min respectively (Fig. 1c). An intense plasmon absorption band at approximately 390 nm is observed for the silver particles. This band signifies that the clusters contain very few silver atoms.

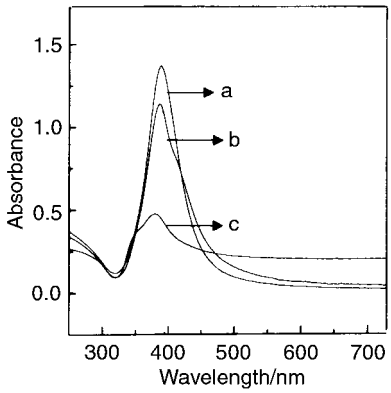

Fig. 1 Optical absorption spectra of silver clusters in aqueous solution: (a) as prepared, (b) after 150 min, (c) after 270 min.

Such a band at 380 nm has already been observed for colloidal particles with a diameter around 1 nm.[23,24] In comparison, our clusters show an average diameter of 0.55 nm as estimated from the half width of the surface plasmon band.[25] As the clusters are uncapped, this plasmon resonance absorption can only provide information about the particle size of the clusters in the sol which, however, cannot be considered as a true measure of the size. Systematic monitoring of the optical absorption of the silver sol every 30 min shows that it is stable only for 120 min. For example, the absorption of the same cluster solution after 150 min (Fig. 1b) shows changes in the shape of the absorption band. Interestingly, the peak maximum is observed at the same wavelength but with reduced intensity. This along with the presence of a red shifted shoulder presumably suggests the deterioration of the cluster solution after two hours. The agglomeration of particles can be distinctly seen as a shoulder appearing at 300 nm in Fig. 1c, although the existence of clusters is apparent by the band at 390 nm which is substantially reduced in intensity. Since size effects limit the lifetime of the clusters in the aqueous solution as reflected by the coalescence, disproportionation and oxidation of clusters,[26] a fresh solution was always prepared for sequential organisation on the SAM covered surface.

III.2 Identification of superlattice formation

Fig. 2 shows the sulfur core level X-ray photoelectron spectrum of a SAM covered gold film. In order to determine the S 2p binding energies as accurately as possible, a non-linear least squares fit of the data was performed using two gaussian pairs consisting of spin–orbit components ($2p_{3/2}$ and $2p_{1/2}$) with a

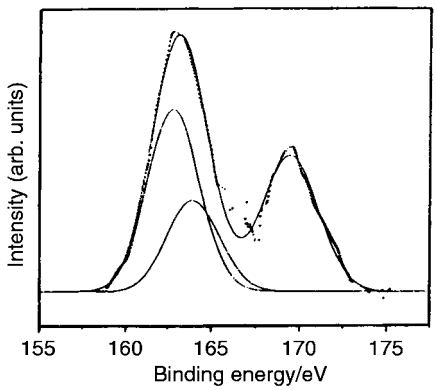

Fig. 2 X-Ray photoelectron spectra for the dithiol functionalized Au surface: S 2p core level region of dithiol monolayer on gold together with non-linear least squares Gaussian fits showing spin–orbit components (*ca.* 163 corresponding to $2p_{3/2}$) with a separation of 1.15 eV and a peak (*ca.* 167 eV) due to sulfate/sulfonic acid moieties.

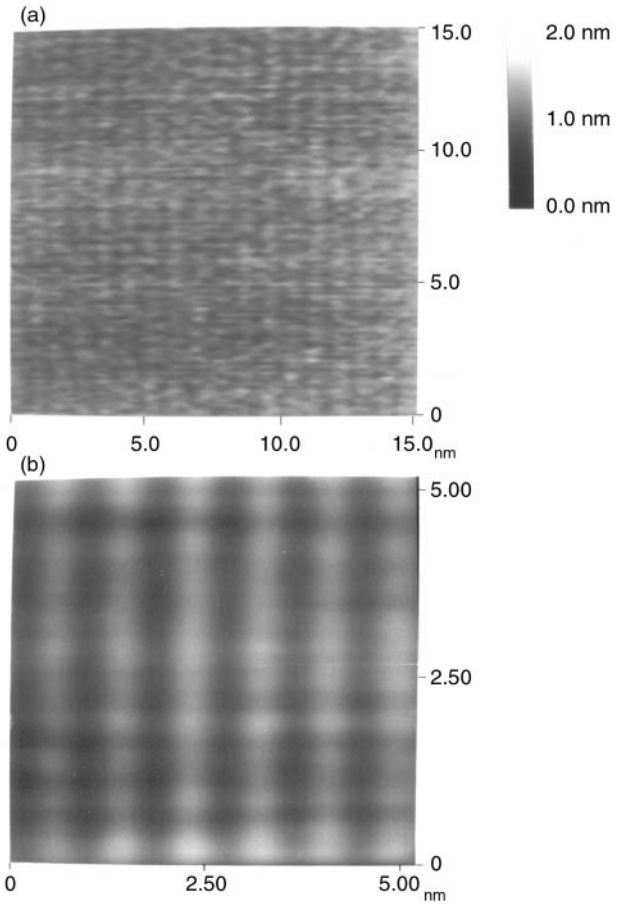

Fig. 3 AFM image of the first layer of silver nanoclusters on SAM coated gold. The images presented contain 256×256 data points collected within several seconds. (a) Raw image, (b) enlarged and Fourier transform-filtered image.

separation of 1.15 eV. The least squares fit indicates that there are two sulfur species separated by ~ 6 eV. The lower peak at *ca.* 163 eV is in good agreement with that reported earlier[27] for chemisorbed thiol and dithiol monolayers on Au and Ag. The second peak at *ca.* 167 eV is thought to be due to sulfate or sulfonic acid moieties[28] formed due to X-ray beam induced damage of free thiols. Both sulfate and sulfonic moieties seem to be present from the XPS as this peak appears more distorted.

The AFM raw image (Fig. 3a) of the first layer of silver clusters obtained after the adsorption of clusters indicates a highly ordered and closely packed array of silver nanoclusters appearing as nanorods in the FT filtered image (Fig. 3b). The protrusions coming out of the radius of the tip are likely to cause an enhancement in the resolution as observed in the present case. This anisotropically ordered arrangement is attributed to the diffusion of the unprotected silver clusters across the SAM, due to strong dispersion interactions between metal clusters. The cluster arrays having a width of ~ 6.5 Å and height of ~ 20 Å are clearly seen in the enlarged and processed image.

Fig. 4 shows the low angle XRD pattern of four layers of Ag nanostructures on a SAM functionalized gold substrate. The diffractogram reveals a significant peak at 2.08° illustrating the sequential organisation of Ag clusters on the SAM surface. This peak corresponding to the longitudinal repeat distance of 42 Å suggests interesting organisational changes in the cluster shape after adsorption on the dithiol template. An approximate calculation of the cluster height from the difference between the assessed periodicity and the dithiol length (*ca.* 9 Å from ellipsometric measurements assuming a refractive index of 1.5 for dithiol SAM) gives 32 Å. Although this estimated cluster

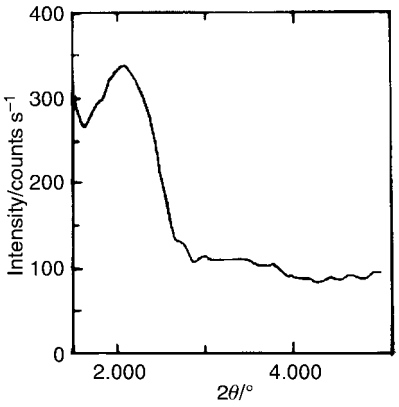

Fig. 4 Low angle X-ray diffractogram of four layers of Ag nanostructures on a SAM functionalized gold substrate taken at a scan rate of 0.5° min^{-1}.

height is considerably larger than that observed in the AFM image, this discrepancy could be attributed to various reasons such as the presence of multiple layers, large errors involved in the ellipsometric measurements of small molecules *etc.*

III.3 Cyclic voltammetry

The processes of adsorption of dithiol and subsequent Ag cluster attachment in various stages have been followed by measuring the cyclic voltammetric response of these modified electrodes in 1 M aqueous KCl solution. Fig. 5 shows such a superimposed cyclic voltammogram of a gold electrode modified with a dithiol SAM (a), and after the adsorption of Ag clusters in two stages (b and c) in the potential range of -1.0 to $+0.8$ V. The significant reduction in capacitance upon SAM formation as manifested in the comparison of the CVs for the bare and SAM covered surfaces has been discussed several times previously.[29] An approximate estimation of the double layer capacitance (at $E = 250$ mV *vs.* SCE) value from this response taken at 500 mV s^{-1} scan rate indicates a capacitance change from 25 μF cm^{-2} for bare gold (not indicated in the figure for clarity) to 1.2 μF cm^{-2} for the dithiol modified gold electrode (Fig. 5a) suggesting the compact nature of the primary monolayer. Two-dimensional organisation of Ag nanoclusters on this primary SAM surface drastically increases the differential capacitance from 1.2 to 35 μF cm^{-2} (Fig. 5b) while a slight decrease is observed for a repeated sequence of SAM formation and Ag nanocluster organisation (Fig. 5c). A geometric variation alone (*i.e.* area under the peak and separation) cannot account for these interesting changes in differential capacitance and perhaps a more important reason

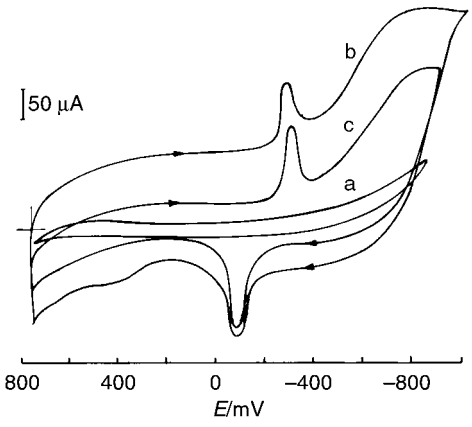

Fig. 5 Superimposed cyclic voltammograms in 1 M KCl for (a) a gold electrode modified with a SAM of 1,5-pentanedithiol, and after (b) one layer and (c) two layers of silver nanocluster superlattice formation on the SAM surface with a typical scan rate of 500 mV s^{-1}.

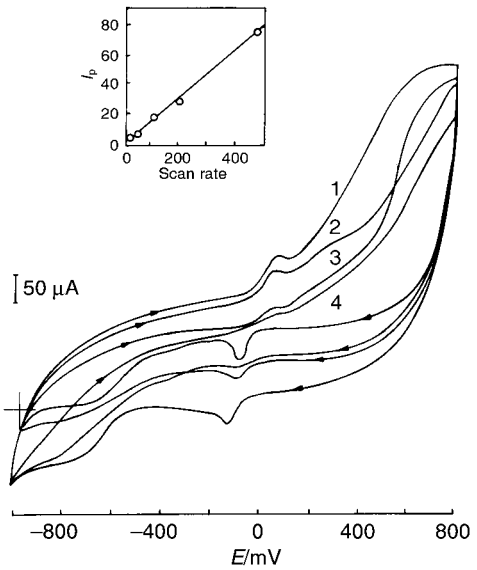

Fig. 6 Cyclic voltammograms of a dithiol functionalized gold electrode with one layer of Ag nanoclusters taken at various scan rates in 1 M aqueous KCl solution in the potential range of −1.0 to +0.8 V. (1) 50, (2) 100, (3) 200 and (4) 500 mV s^{-1}.

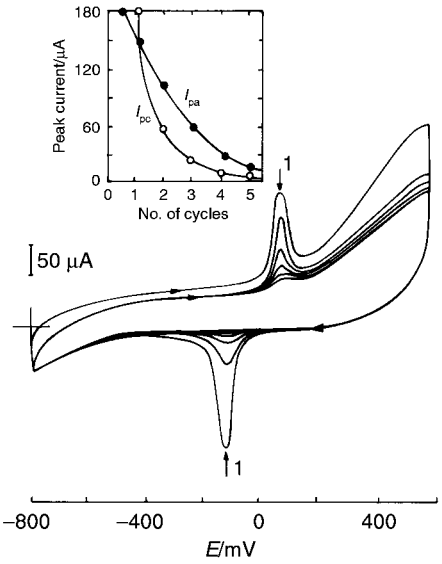

Fig. 7 Cyclic voltammogram for a two layer assembly of ordered nanostructures on a dithiol modified gold electrode at 200 mV s^{-1} in the potential range of −1.0 to +0.8 V for five successive cycles.

is the abrupt change in dielectric constant before and after silver nanocluster formation.

Consequently more importance should be given to the presence of a sharp reversible peak after Ag nanocluster organisation, which in combination with the above change in double layer capacitance suggests that Ag clusters act as a nanoelectrode array collectively enabling the passage of electrons through the SAM barrier. Although the blocking effect of the SAM is retained in the anodic region of Fig. 5b, a sharp reversible peak is observed around $E^{\circ} = -100$ mV *vs.* SCE with a peak to peak separation of 190 mV and a peak current ratio approaching unity. Apart from demonstrating the redox accessibility of Ag nanoclusters, a comparison of this formal potential with the standard value corresponding to the Ag/Ag^{+} couple (+0.779 *vs.* SCE) suggests the importance of quantum size effects.[23] Since the silver clusters are surface bound, one ideally expects all the characteristic signatures of voltammetric response of an electrochemically reversible redox reaction (peak current, I_p, proportional to scan rate; peak potentials and wave shapes for the cathodic and anodic surfaces identical and the full width at half maximum (FWHM) equal to $90.61/n$ mV, where n is the number of electrons transferred) although deviations due to non-idealities such as particle–particle and adsorbed particle–organic dipole interactions can occur.

Organisation of the second layer of Ag nanoclusters (Fig. 5c) does not change the position of both the peaks and this similarity of $E_{1/2}$ values also suggests that the size of the Ag nanoclusters in the second layer is not drastically different from the size in the first layer. The full widths at half maximum are also identical but the actual peak current and coverage for both oxidation and reduction peaks for the second layer are more (*e.g.* the calculated coverage values of the cathodic peak for second and first layers are 30.3 μC cm^{-2} and 25.1 μC cm^{-2} respectively). An approximate calculation of the charge under the peak for both the first and second layers also shows less charge for the anodic peak, probably due to electrostatic repulsion between the oxidised form of clusters.

Fig. 6 shows the cyclic voltammograms of a dithiol monolayer with one layer of Ag nanoclusters taken at various scan rates (without any correction due to ohmic drop) in 1 M aqueous KCl solution in the potential range of −1.0 to +0.8 V. The reversible redox couple can be observed at all scan rates, although a 100 mV s^{-1} scan rate gives optimum features of highest peak current and lowest peak potential separation. Compared to the anodic peak potentials, the cathodic peak potentials are found to shift more with scan rate and a stronger binding of thiols to the reduced form of the clusters may be one of the contributing factors. The inset of Fig. 6 shows that the voltammetric peak current is proportional to the potential scan rate, which is consistent with the expectation that the silver clusters are surface bound. Further confirmation arises from the diminishing separation between the anodic and cathodic peaks (ΔE_p) as the scan rate decreases. Comparison of the observed FWHM with the theoretically expected value of $90.61/n$ mV suggests the involvement of two electrons in the redox reaction of the clusters if the theory of the voltammetric response for the surface wave is applicable. Beyond the anodic peak corresponding to silver cluster oxidation, the increase in background current can be explained by the slow oxidation of the dithiol molecules.

The high degree of reversible behaviour observed at 200 mV s^{-1} ($I_{pa}/I_{pc} \approx 1$, $\Delta E_p = 45$ mV) is found to be adversely affected by repeated cycling. For example, Fig. 7 shows cyclic voltammetric data for a two-layer assembly of ordered nanostructures at this scan rate for five successive cycles. Although diminishing peak currents with increasing number of cycles have been observed for both anodic and cathodic peaks (see inset Fig. 7) there is an important difference. The decrease for the cathodic case is more abrupt (*e.g.*: 1st to 2nd to 3rd cycle) compared to the anodic case which could be attributed to many reasons such as different electrostatic surface potentials of the clusters, rearrangement of thiol molecules on the surface, the possibility of destruction of the SAM by reductive desorption, *etc.* As the number of cycles increases, there can be a significant loss of Ag clusters to solution and the final shape in the anodic side suggests a plateau current possibly due to the presence of large defects (microelectrode behaviour). Approximate calculation of the area under the peak (20–30 μC cm^{-2}) for the voltammogram taken at 100 mV s^{-1} provides the accessible concentration of Ag clusters as more for cathodic, perhaps due to the increased amount of oxidised clusters accessible for reduction. The reversible peak in the initial few cycles clearly indicates that protected Ag clusters act as an array of nanoelectrodes enabling the passage of electrons through the SAM barrier.

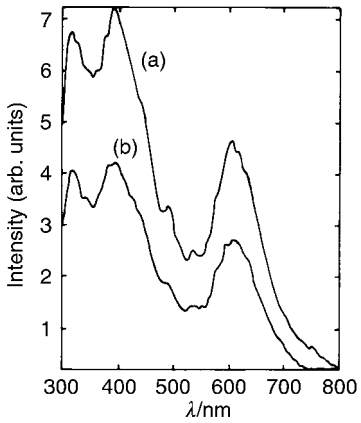

Fig. 8 Photoluminescence spectra of (a) two layers and (b) four layers of Ag nanocluster superlattices on a SAM functionalized surface taken at room temperature (not corrected for the instrument).

III.4 Photoluminescence studies

Fig. 8 shows the room temperature emission spectra of silver cluster superlattices of two and four layers. The superlattice structure manifests a conventional quantum well structure. The electronic charge distribution then can be expected to be delocalized along the direction normal to the well layer,[30] for the barrier thickness (here dithiol thickness of ~ 9 Å) is sufficiently small to allow electronic coupling between wells. Owing to this coupling the broadening of the quantized electronic states of the wells occurs giving rise to new broadened and delocalized quantized states called minibands. The three distinct transitions in the emission spectra at 320, 400 and 620 nm manifest as minibands in the superlattice structure whereas the silver cluster solution exhibits no such bands. This is also probably one of the reasons for the observation of efficient charge transport normal to the layers as in agreement with the presence of sharp peaks in the CV. No significant change in the PL spectrum has been observed with the number of layers, which is consistent with the above explanation.

IV. Conclusions

These results imply a methodology for the sequential organisation of self-assembled monolayers and highly ordered silver nanocluster arrays from aqueous solution to form a superlattice structure at room temperature. In particular, this type of layer-by-layer deposition of arrays of silver clusters on a dithiol SAM overcomes several diffusional and orientational restrictions to form finally a nanorod like superstructure as indicated by AFM imaging. It also raises a subtle question about the acquired order and electron coupling across the barrier, especially in modulating the optoelectronic properties as manifested in the PL behaviour. The mechanism of electron transfer (tunnelling or hopping) also needs further investigation since the silver clusters can be addressed electrochemically as demonstrated by the accessibility of silver nanoclusters for redox behaviour.

Acknowledgements

One of the authors, S. P., would like to thank CSIR, India for financial support. M. A. thanks CSIR, New Delhi for a Senior Research Fellowship. The authors would like to thank Centre Director, IUC-DAEF, Indore for providing the AFM facility.

References

1 C. P. Collier, T. Vossmeyer and R. J. Heath, *Annu. Rev. Phys. Chem.*, 1998, **49**, 371.
2 S. A. Harfenist, Z. L. Wang, R. L. Whetten, I. Wezmar and M. M. Alvarez, *J. Phys. Chem.*, 1996, **100**, 13904.
3 R. Elghanian, J. J. Storhoff, R. C. Munic, L. R. Letsinger and C. R. Mirkin, *Science*, 1997, **277**, 1078.
4 T. Nakanishi, B. Ohtani and K. Uosaki, *J. Phys. Chem. B*, 1998, **102**, 1571.
5 C. R. Kagan, C. B. Murray and M. G. Bawendi, *Phys. Rev. B*, 1996, **54**, 8633.
6 A. A. Guzelian, J. E. B. Katari, A. V. Kadavanich, U. Banin and K. Hamad, *J. Phys. Chem.*, 1996, **100**, 7212.
7 J. S. Yin and Z. L. Wang, *Phys. Rev. Lett*, 1997, **79**, 2570.
8 C. N. R. Rao, G. U. Kulkarni, P. J. Thomas and P. P. Edwards, *Chem. Soc. Rev.*, 2000, **29**, 27.
9 Z. L. Wang, S. A. Harfenist, R. L. Whetten, J. Bentley and N. D. Evans, *J. Phys. Chem. B*, 1998, **102**, 3068.
10 M. M. Alvarez, J. T. Khoury, T. G. Schoatt, M. N. Shafigullin, I. Vezmar and R. L. Whetten, *J. Phys.Chem. B*, 1997, **101**, 3706.
11 C. B. Murray, C. R. Kagan and M. G. Bawendi, *Science*, 1995, **270**, 1335.
12 K. S. Mayya and M. Sastry, *Langmuir*, 1999, **15**, 1902.
13 B. A. Korgel and D. Fitzmaurice, *Adv. Mater.*, 1998, **10**, 661.
14 M. D. Musick, C. D. Keating, L. A. Lyon, S. L. Botsko, D. J. Pena, W. D. Holliway, T. M. McEvoy, J. N. Richardson and M. J. Natan, *Chem. Mater.*, 2000, **10**, 2869.
15 K. Vijayasarathi, P. J. Thomas, G. U. Kulkarni and C. N. R. Rao, *J. Phys. Chem. B*, 1999, **103**, 399.
16 A. Taleb, V. Russier, A. Courty and M. P. Pileni, *Euro. Phys. J. B*, 1999, **59**, 13350.
17 U. Simon, R. Flesch, H. Wiggers, G. Schon and G. Schmid, *J. Mater. Chem.*, 1998, **8**, 517.
18 J. R. Heath, C. M. Knobler and D. V. Leff, *J. Phys. Chem. B*, 1997, **101**, 189.
19 P. C. Ohara, J. R. Heath and W. M. Gelbart, *Angew. Chem.*, 1997, **36**, 1078.
20 K. Bandyopadhyay, M. Sastry, V. Paul and K. Vijayamohanan, *Langmuir*, 1997, **13**, 866.
21 K. Bandyopadhyay and K. Vijayamohanan, *Langmuir*, 1998, **14**, 6924.
22 *Clusters and Colloids*, ed. G. Schmid, VCH, New York, 1994.
23 A. Henglin, *J. Phys. Chem.*, 1993, **97**, 5457.
24 M. Mostafvi, N. Keghouche, M. Delcourt and J. Belloni, *Chem. Phys. Lett.*, 1990, **167**, 193.
25 U. Kreibig and L. Genzel, *Surf. Sci.*, 1985, **156**, 678.
26 M. Brust, J. Flink, D. Bethell, D. J. Schiffrin and C. J. Kiely, *J. Chem. Soc., Chem. Commun.*, 1995, 1655.
27 D. G. Castner, K. Hinds and D. W. Grainger, *Langmuir*, 1996, **12**, 5083.
28 Z. Mekhalif, J. Riga, J. J. Pireaux and J. Delhalle, *Langmuir*, 1997, **13**, 2285.
29 C. Miller, P. Cuendet and M. Grätzel, *J. Phys. Chem.*, 1991, **95**, 877.
30 A. J. Nozik, C. A. Parsons, D. J. Dunlavy, B. M. Keyes and R. K. Ahrenkiel, *Solid State Commun.*, 1990, **75**, 297.